EXPERIMENTAL STUDY OF STRAIN GRADIENT EFFECT ON THE BEHAVIOUR AND STRENGTH OF MASONRY

J. Hou[1], Y. Liu[2] and J. Dawe[3]
[1]Former MASc student, Dept of Civil Engineering, Dalhousie University, Halifax, NS, Canada
[2]Associate Professor, Dept of Civil Engineering, Dalhousie University, Halifax, NS, Canada
[3]Professor, Dept of Civil Engineering, University of New Brunswick, NB, Canada

SUMMARY

Forty-two masonry prisms including both grouted and hollow specimens were tested under different loading conditions to investigate the strain gradient effect on masonry. Results showed that failure modes were associated with applied eccentricities and a reduction in load capacity as a result of an increase in eccentricity is more significant for grouted prisms than for their hollow counterparts. At a relatively large eccentricity to thickness ratio, *e/t*, hollow prisms attained a higher ultimate load than grouted prisms. The strain gradient effect increases with an increase in the eccentricity for grouted prisms but the increase is marginal for hollow prisms. Specimens loaded under double curvature bending showed higher strain gradient effect than was evident for those loaded in single curvature bending.Coefficients for the equivalent stress distribution block based on experimental stress-strain curves were obtained for prisms under eccentric loading. An evaluation of the rectangular stress block used in both American and Canadian design codes showed that the rectangular stress block provides adequate and somewhat conservative estimate of masonry compressive strength and this conservatism increases as the strain gradient effect increases.

INTRODUCTION

In practice, a large portion of masonry elements are required to resist combined axial load and out-of-plane bending, whether it is due to wind, earthquake or eccentricity of the axial compressive load. The moment causing out-of-plane bending is commonly described as an axial load with a virtual eccentricity e. The cross-sectional strength of these structural elements is governed by the simultaneous interaction of axial load resistance and moment capacity. The associated strength curve is referred to as the P-M interaction diagram. Previous research has shown that the capacity of masonry prisms decreases with an increase in eccentricity and therefore eccentricity coefficients were developed to relate the capacity at various eccentricities to the capacity at zero eccentricity (SCPI 1969; Drysdale et al. 1994). However, Turkstra and Thomas (1978) and Drysdale and Hamid (1983) found that based on linear elastic analysis and assuming zero tensile strength, for prisms made with solid units, the calculated maximum compressive stress at the extreme fibre at failure was significantly higher than the compressive strength obtained from concentric loading. This increase in compressive strength has been referred to as the strain gradient effect. However, for hollow masonry units, the increase in compressive stress at the extreme fibre is small. Other researchers (Yokel et al. 1971; Brown and

Young 1988; Maurenbrecher 1983) have reported similar observations in their experimental findings. The compression strength gain has been attributed to a smaller part of the mortar joint being under high stresses, which in turn results in lower lateral tensile stresses in masonry units (Hilsdorf 1969). In working stress design, the strain gradient effect has been included in design codes by either increasing the theoretical eccentricity coefficient by some amount or specifying a higher allowable stress due to flexure compared to allowable stress due to axial compression (CSA S304-M78 1978). With the implementation of strength design method, both American design code (ACI 530-05/ASCE 5-05/TMS 402-05) and Canadian design code (CSA S304.1-04) recommend the use of a nonlinear stress-strain relationship for masonry in compression obtained from concentric loaded prisms to evaluate the compressive force provided by masonry. The implicit assumption is that the strain gradient does not affect the shape of stress-strain relationship. For practical design, both codes suggest that the non-linear stress distribution can be simplified as an equivalent rectangular stress block for masonry cross-section under combined axial and bending. Adopted from Whitney stress block theory used in concrete design (Hognesd et al. 1955), this method ignores tensile strength in masonry and uses the product of a coefficient and the specified f'_m obtained from conventional concentrically loaded prism tests as the flexural compressive strength. While the American code prohibits the design of masonry beam-columns subject to axial loads greater than $0.2\ f'_m A_g$ where A_g is the gross cross-sectional area of a masonry member, there are no similar restrictions on the design axial load in the Canadian code. A review of this topic indicated that while the current design codes recommend the use of rectangular stress block theory to account for strain gradient effect, its effectiveness in masonry application has not yet been fully investigated.

An experimental program was therefore designed and conducted to investigate the strain gradient effect on the capacity and behaviour of masonry prisms under eccentric compressive loading. Both hollow and grouted prisms were included in the study and the experimental results were used to evaluate the effectiveness of rectangular stress block theory in masonry under strain gradient.

TEST SPECIMENS

Forty-two 5-course high plain masonry prisms were tested in 3 series under compressive loading with varying eccentricities. A detailed description of prism specimens is presented in Table 1. Both hollow and grouted prisms designated as “H” and “G” were tested in Series A, B and C. Series A specimens were tested under a concentric axial load as control specimens to obtain the stress-strain relationship and compressive strength of masonry in pure compression. Series B and C specimens were tested under eccentric compressive loading causing single curvature bending and double curvature bending, respectively. For each tested parameter combination, three tests were conducted. The applied eccentricities, *e*, for each specimen are also listed in Table 1.

All specimens were constructed in stack bond pattern using standard two-core concrete blocks with dimensions of 390x190x140 mm. Type N ready-mix mortar was used in laying up the specimens. For hollow specimens, the bed joint mortar was applied only to the face shells while it was applied to both face shells and webs for grouted specimens. No.9 ASWG ladder type joint reinforcement was placed in alternate courses of each prism at a spacing of 400 mm center to center. Along with test specimens, auxiliary tests were conducted to evaluate material properties of the masonry constituents including blocks, mortar, and grout.

Table 1 Test results of specimens

Specimen	No. of spec.s	*e/t*	Average ultimate load, P_u (kN)	Average deflection at P_u Δ_u (mm)	Total moment M_u (kN-m)
AG	3	0	579	0.04	-
AH	3	0	359	0.03	-
BG-1	3	1/6, 1/6	337	0.9	8.2
BG-2	3	1/4, 1/4	260	1.3	9.4
BG-3	3	1/3, 1/3	177	1.7	8.6
BH-1	3	1/6, 1/6	267	0.6	6.4
BH-2	3	1/4, 1/4	231	0.8	8.3
BH-3	3	1/3, 1/3	209	1.0	10.0
CG-1	3	1/6,-1/6	411	0.6	9.8
CG-2	3	1/4,-1/4	315	0.8	11.0
CG-3	3	1/3,-1/3	216	1.1	10.1
CH-1	3	1/6,-1/6	330	0.3	7.8
CH-2	3	1/4,-1/4	305	0.4	10.7
CH-3	3	1/3,-1/3	257	0.6	12.0

TEST SET-UP AND PROCEDURE

The test set-up is shown in Fig. 1. An existing testing frame with a design capacity of 2100 kN was used to act as the reaction frame. Vertical loading was applied using two hydraulic rams with a capacity of 900 kN each through a loading beam. For safety reason, two hydraulic rams were placed on the strong floor and centered with respect to both longitudinal and transverse centrelines of the prism. Each specimen was housed in two channels at two ends. Pinned-pinned support conditions were adopted for all tests. In order to counteract the potential twisting force of the specimen during the test, the lateral movement of specimens at both ends was restrained. As shown in Fig. 1, knife edge plates were placed against both the top loading plate and the flanges of bottom loading beam, which allowed vertical movement but prevented the lateral movement of the loading plate and beam.

Vertical deformations and lateral deflections were measured using linear variable differential transducers (LVDT). All LVDTs were calibrated to read in increments of 0.001mm. Lateral deflections were measured at the theoretically determined maximum lateral deflection location. To eliminate any errors due to twisting of a specimen, lateral deflections were measured at both front and back of the specimen at appropriate locations and the average value of two measurements was used for the analysis. For Series A and B specimens, lateral deflections were measured at mid-height of each specimen. For Series C specimens subjected to double curvature bending, the calculated maximum lateral deflection location was determined to be at locations of 0.21L and 0.79L along the specimen height. Therefore, the measurements were taken at these locations in the vicinity of the mortar joint between the 3rd and 4th course from the top and

bottom of a prism. Corresponding to the lateral deflection location, vertical deformations were measured and used to calculate the vertical strains on both tension and compression faces of the prisms.

Prior to each test, the prism was centered in the test position and vertically and transversely aligned with the assistance of a laser level. The specimen was then cycled twice using nominal load of 10% of the predicted ultimate load to ensure that the specimen and instrumentation were properly seated before beginning a test. During each test, vertical load was applied gradually at a rate of about 50 kN per minute until ultimate compression failure occurred. Failure was considered to have occurred when the specimens displayed large lateral deflections at decreasing applied loads. Vertical loads, vertical deformations and lateral deflections were measured and recorded using an electronic data acquisition system throughout the loading history.

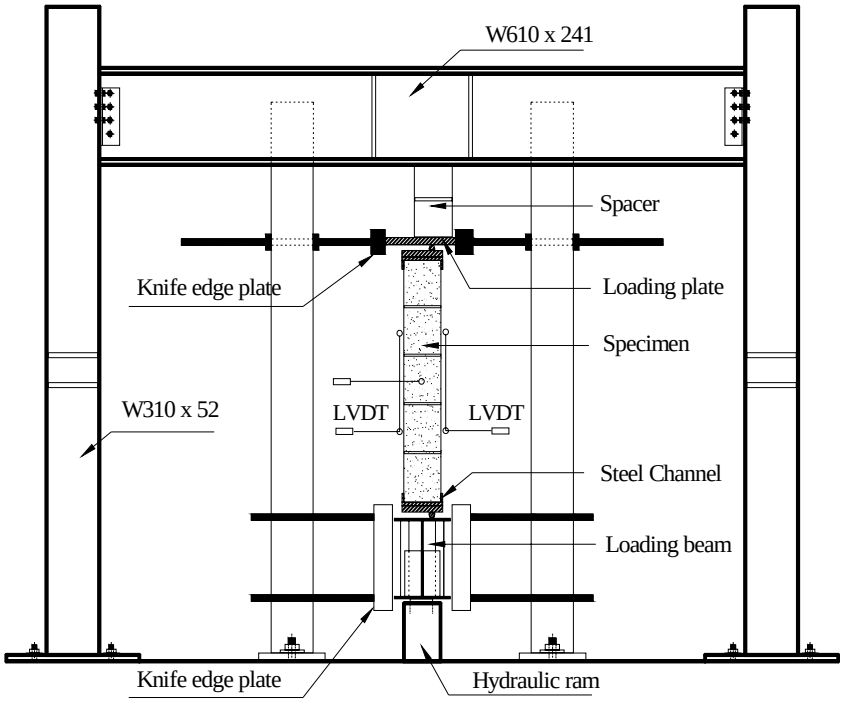

Fig. 1 Test set-up

ANALYSIS AND DISCUSSION OF TEST RESULTS

Failure Mode

Associated with loading and grouting conditions, three failure modes including compression, combined compression and tension, and tension failure were observed. For Series A specimens, the failure mode was a typical compression failure initiated by vertical splitting cracks through both the web and faceshells of specimens as shown in Fig. 2. For grouted specimens in Series B and C, as e/t ratio increased from $t/6$ to $t/3$, the failure mode shifted from compression characterized by vertical splitting cracks and masonry crushing to tension controlled failure initiated by tensile cracking with no evidence of masonry crushing. However, for hollow specimens tested at $e=t/3$, the failure was more of a compression controlled failure without

significant tensile cracking as shown in Fig. 3. This is attributed to a greater kern eccentricity for the hollow cross-section than that of a grouted cross-section. The failure for majority double curvature specimens was initiated very close to the bottom or the top of the specimen for all tested eccentricities.

Fig. 2 Failure mode of specimen AG-1

Fig. 3 Failure mode of specimen BH-3 (e/t =1/3)

Ultimate Load

Results of tested specimens are summarized in Table 1, where P_u is the average ultimate compressive load, Δ_u is the measured maximum lateral deflection occurring at P_u and M_u is the total moment including secondary moment effect. As seen in the table, for Series A specimens tested under a concentric compressive loading, the average ultimate load was 579 kN for grouted specimens which is about 61% higher than that of hollow specimens. The lateral deflections, Δ_u, at P_u are small with a magnitude of less than 0.1 mm for both types of specimens as expected for concentric loading cases. It is evident that as the eccentricity increases, the ultimate load and the stiffness at failure decrease while the ductility increases resulting in increased ultimate deflection for both types of specimens. However, the rate of reduction of ultimate load varies. As the eccentricity increased from $t/6$ to $t/3$, the ultimate load decreased 22% for hollow specimens while this decrease was approximately 47% for fully grouted prisms. Referring to results for both Series A and B specimens, fully grouted specimens attained 1.61, 1.26 and 1.12 times the ultimate capacities of hollow specimens when the applied eccentricity was 0, $t/6$ and $t/4$. However, at eccentricity of $t/3$, the hollow specimens BH-3 attained an ultimate load of 209 kN, which is about 18% higher than fully grouted specimens BG-3 with a capacity of 177 kN. This paradox is attributed to different failure modes associated with the two types of specimen. At e/t =1/3, the hollow specimens failed primarily by masonry crushing with a large area being in compression while the grouted specimen failure by tension initiated by opening up of the mortar joint and followed by collapse of the specimen.

A comparison of results in Series B and C in Table 1 shows that specimens in Series C attained consistently higher ultimate loads than those in Series B tested under the same eccentricity. Among specimens in Series C, a similar trend where the reduction of capacity for fully grouted specimens is more significant than that of hollow specimens is also observed. Also, at an eccentricity of *t/3*, the hollow specimens attained higher ultimate load than the grouted specimens. This seems to indicate that with an increase in eccentricity, the advantage of grouting in providing extra strength diminishes. The maximum lateral deflections increased with an increase in eccentricities for both Series B and C specimens while the magnitudes for Series C specimens were significantly lower than those of Series B. For both series, fully grouted specimens experienced greater lateral deflections than hollow specimens tested under the same applied eccentricity.

Strain Gradient Effect

Calculated compressive stresses at extreme fibre

To evaluate the strain gradient effect, a linear elastic analysis and zero tensile strength assumption for masonry were adopted to calculate the compressive stress at the extreme compression fibre of tested prisms. Table 2 presents the results of calculated compressive stresses, f_{me}, at extreme compressive fibre taking into account lateral deflections for all specimens. For Series A, the average stresses for 3 grouted and 3 hollow prisms were calculated simply by dividing the ultimate load by the effective cross-sectional area. For the remaining specimens, the ratio of calculated compressive stress, f_{me}, at the extreme fibre to the average stress, f_m, obtained in Series A specimens, defined as the flexural compressive stress factor "*a*", is also listed in the table. The procedure for calculating f_{me} at the extreme fibre takes into account of development of cracking through the depth of the cross section. A similar method is also illustrated by Drysdale and Hamid (1983). It is confirmed that the strain gradient effect exists where the calculated flexural compressive stress factor "*a*" is greater than 1.0.

Figure 4 illustrates the relationship between the flexural compressive strength factor "*a*" and *e/t* ratios for both grouted and hollow specimens. It shows that in general, flexural compressive strength factor *a* increases with the increase of *e/t* ratios while this increase is more significant for grouted specimens than for hollow specimens. For example, for the same *e/t* ratio increase from 1/6 to 1/3, the increase of *a* was determined to be approximately 10.9% and 1.8% for grouted and hollow specimens respectively, and 9.0% and 1.4% for grouted and hollow specimens in Series C respectively. As shown in Fig.4, the factor "*a*" is also affected by loading conditions. Series C specimens loaded in double curvature bending demonstrated higher "*a*" values and thus a greater strain gradient effect than those in Series B loaded in single curvature bending. The higher "*a*" values are believed to be directly associated with the higher ultimate loads attained by specimens in Series C.

Stress-strain relationship

To evaluate the strain gradient effect on the stress-strain relationship for masonry in compression, the stress-strain curves of specimens in Series A, B and C were determined. The average strains were calculated using vertical deformation within a gauge length measured on the specimen compressive face at the maximum lateral deflection location. The calculated compressive stresses at the extreme compressive fiber, f_{me}, were plotted as compressive stresses.

Table 2 Results of strain gradient effect and stress block coefficients

Specimen	*e/t*	P_u (kN)	Calculated maximum stress, f_{me} (MPa)	Flexural compressive strength factor, *a*	Stress block coefficients k_1k_3 & (k_2)	Ultimate strain, ε_u
AG	0	579	10.6	1.00	0.590 (0.310)	0.00156
AP	0	359	15.7	1.00	-	0.00147
BG-1	1/6, 1/6	337	12.6	1.19	0.703(0.382)	0.00253
BG-2	1/4, 1/4	260	13.3	1.25	0.731(0.402)	0.00293
BG-3	1/3, 1/3	177	14.0	1.32	0.763(0.408)	0.00325
BH-1	1/6, 1/6	267	17.6	1.12	-	0.00208
BH-2	1/4,1/4	231	17.8	1.14	-	0.00210
BH-3	1/3,1/3	209	17.9	1.14	-	0.00221
CG-1	1/6,-1/6	411	15.2	1.44	0.715(0.446)	0.00234
CG-2	1/4,-1/4	315	16.0	1.51	0.777(0.464)	0.00241
CG-3	1/3,-1/3	216	16.6	1.57	0.843(0.490)	0.00255
CH-1	1/6,-1/6	330	21.6	1.38	-	0.00197
CH-2	1/4,-1/4	305	22.0	1.40	-	0.00202
CH-3	1/3,-1/3	257	22.0	1.40	-	0.00211

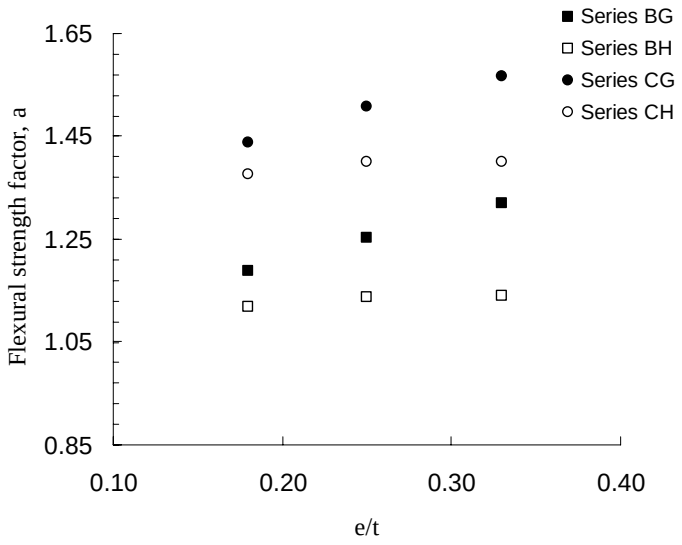

Fig. 4 Flexural compressive strength factor *a* vs. *e/t* ratio

Figures 5 and 6 show comparisons of stress-strain curves between Series B and C specimens and conventional stress-strain curves of Series A specimens for both grouted and

hollow prisms. For Series B grouted specimens, the stress-strain curves demonstrated evident non-linearity at increasingly earlier loading stage as eccentricity varied from *t*/6 to *t*/3. For hollow specimens, the stress-strain curves for all tested eccentricities remained linear up to 90% of the ultimate load, indicating the strain gradient had little effect on the shape of the stress-strain curve for hollow prisms. A comparison of stress-strain curves between eccentrically and concentrically loaded specimens indicates that the shapes of stress-strain curves in general are similar while the eccentrically loaded specimens showed more pronounced non-linear behaviour. The average ultimate strains for each specimen are listed in Table 2. As expected, the eccentrically loaded specimens attained ultimate strains in a range of 0.0021 and 0.0033, which is higher than that of concentrically loaded specimen. For specimens tested in Series C, the shape of stress-strain curve between concentrically and eccentrically loaded specimens remained similar. However, noticeable variation is more evident for both grouted and hollow specimens compared with curves obtained for Series B specimens. Resulting from a higher degree of strain gradient effect, this variation may lead to a significant discrepancy between the experimental and code suggested capacity, which is based on stress-strain relationships for concentrically loaded prism tests.

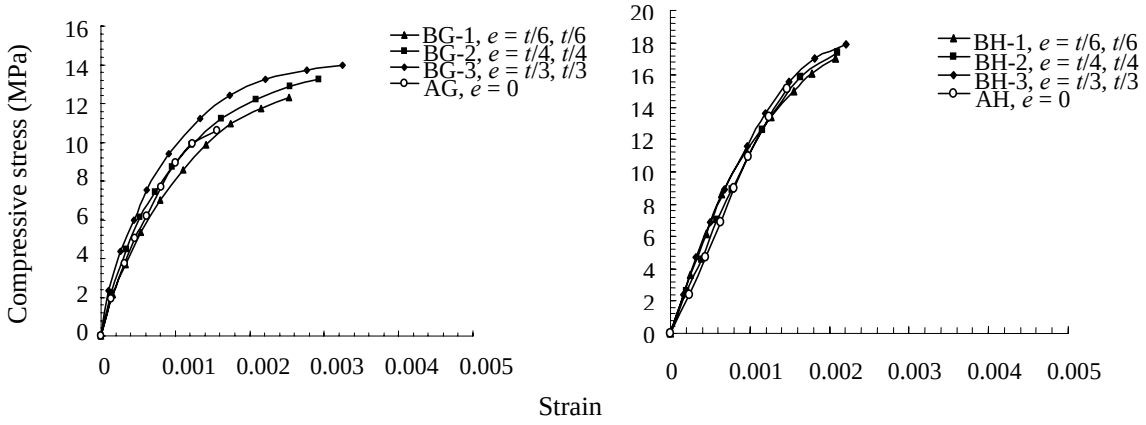

Fig. 5 Stress-strain curves for Series B specimens

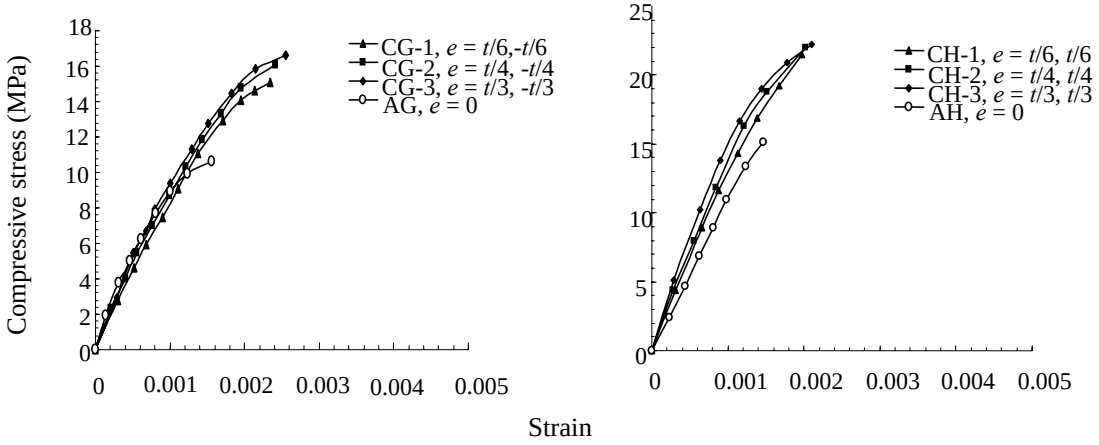

Fig. 6 Stress-strain curves for Series C specimens

Comparison with Current Design Codes

The current masonry design codes in Canada and America recommend the use of rectangular stress block theory to evaluate the resistance of masonry members under combined axial and out-of-plane bending. The flexural strengths for the equivalent rectangular stress distribution are specified to be $0.85\,f'_m$ in the Canadian code and $0.80\,f'_m$ in the American code. In addition, both codes permit the use of stress-strain curves of any shape that result in prediction of strength in substantial agreement with the results of experimental tests. To evaluate the efficacy of rectangular stress block theory, stress-strain curves shown in Figs. 5 and 6 for grouted prisms were used to obtain values of k_1k_3 and k_2 where k_1k_3 is the coefficient for the compressive force and k_2 defines the location of the compressive force. The results are listed in Table 2 and plotted in Fig. 7. It is evident that grouted prisms tested under eccentric loading showed higher values for k_1k_3 than those tested under concentric loading. As the eccentricity increased, a steady increase in the value of k_1k_3 is evident. This seems to indicate that strain gradient does affect the stress block in that the compressive force evaluated using stress-strain curve of grouted masonry under eccentric loading is greater than that evaluated using stress-strain curve for concentric loading. Also seen from Fig. 7, the variation of k_2 values with an increase in eccentricity is not as pronounced. This further confirms that the shape of stress-strain curve is consistent for concentric and eccentric compression. Figure 8 compares the P-M interaction diagram constructed based on the rectangular stress block theory using both codes and experimental average axial loads and corresponding moments for grouted and hollow specimens. In the calculation of the compressive force, it is recognized that the grouted core is weaker than the faceshell for grouted prisms, a more accurate evaluation would require the use of individual compressive strength. However, both codes permit the use of an averaged compressive strength obtained from prism testing for P-M interaction diagram. The variation between two code curves in the compression controlled failure region is a result of different coefficients used for the flexural strength of the stress block. It is noted that the rectangular stress block method, in general, provides adequate and somewhat conservative predictions of cross-sectional strength for both hollow and grouted prisms when single curvature bending is concerned. For specimens in Series C, the underestimation of cross-sectional strength is more significant than that for Series B specimens, especially in the region where compression failure or combined compression and

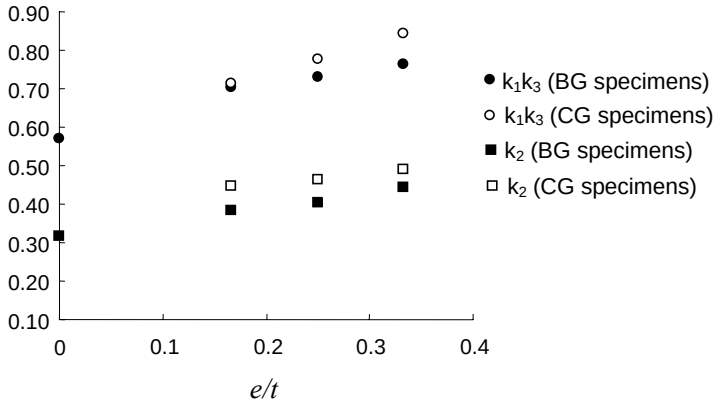

Fig. 7 Results of $k_1\,k_3$ and k_2 for grouted prisms

tension failure predominates. This observation is quite logical considering that coefficients in rectangular stress block method were calibrated based on test results of specimens under eccentric compressive loading causing single curvature bending. It also indicates that the conservatism is most pronounced for specimens demonstrating high flexural strength factor "*a*" and thus high strain gradient effect.

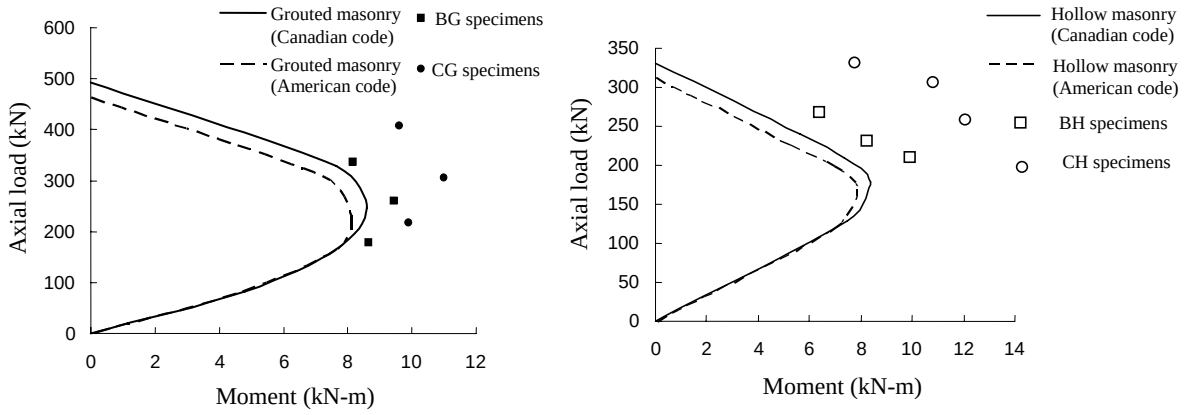

(a) Grouted masonry (b) Hollow masonry

Fig.8 Comparison of P-M diagram and experimental results

CONCLUSIONS

Strain gradient effect on the strength and stress-strain relationship of masonry prisms subjected to combined axial loads and out-of-plane bending conditions has been investigated. The following conclusions may be drawn as a result of this research:

1. The reduction in load capacity as a result of an increase in eccentricity is more significant for grouted masonry than for their hollow counterparts. At an *e/t* ratio of 1/3, for eccentric compressive loads causing single curvature bending, hollow specimens attained higher ultimate load than grouted specimens.

2. Strain gradient effect exists for specimens subjected to loading conditions as investigated in this research. For grouted specimens, the flexural compressive strength factor "*a*" increases with an increase in *e/t* ratios. However, this increase is not as noticeable in the case of hollow specimens.

3. Strain gradient does not have a significant effect on the shape of stress-strain relationship for investigated eccentricities.

4. The rectangular stress block method in both American and Canadian codes provides satisfactory and somewhat conservative estimate of the cross-sectional strength of masonry prisms under single curvature bending. However, the code is markedly conservative for prisms subjected to double curvature bending. The underestimation in masonry strength by the code is most evident for prisms with high strain gradient effect.

Due to laboratory limitations, the number of specimens and parameters investigated in this research are limited. Further investigation involving more geometrical and material properties of specimens are necessary for a conclusive recommendation with regard to the effect of grouting and validity of the rectangular stress block method. It is believed that useful information,

including the behaviour and strain gradient effect of masonry prisms under combined axial load and bending was obtained.

ACKNOWLEDGEMENTS

The authors wish to recognize the contribution of financial assistance by the Natural Sciences and Engineering Research Council of Canada and in kind assistance from the Shaw Group, Nova Scotia, Canada.

REFERENCES

Brown, R.H., and Young, J.M. 1988. Compressive stress distribution of grouted hollow clay masonry under strain gradient. Report No. 1.2 (b)-1, U.S.-Japan Coordinated Program for Masonry Building Research, Department of Civil Engineering, Clemson University, Clemson, SC.

Building Code Requirements for Masonry Structures. 2005. ACI 530-05/ASCE 5-05/TMS 402-05. Masonry Standards Joint Committee, US.

Drysdale, R.G., and Hamid, A.A. 1983. Capacity of concrete block masonry prisms under eccentric compressive loading. Journal of the American Concrete Institute, **80**(01): 102-108.

Drysdale, R.G.., Hamid, A.A., and Baker, L.R. 1994. Masonry Structures: Behavior and Design. Prentice-Hall Inc., Englewood Cliffs, New Jersey.

Hilsdorf, H. K. 1969. An investigation into the failure mechanism of brick masonry under axial compression. Designing, Engineering and Construction with Masonry Products, F. B. Johnson, ed., Gulf Publishing, Houston, pp. 34–41.

Hognestad, E., Hanson, N. W., and McHenry, D. 1955. Concrete stress distribution in ultimate stress design. Journal of the American Concrete Institute, **52**(04): 455-480.

MacGregor, J. G. and Bartlett, F. M. 2000. Reinforced Concrete - Mechanics and Design, 1st Canadian Edition. Prentice Hall Inc., Englewood Cliffs, New Jersey.

Masonry Design and Construction for Buildings. 1978. CSA S304-78. Canadian Standards Association, Rexdale, Ontario, Canada.

Masonry Design for Buildings (Limit States Design). (2004) “CSA S304.1-04”, Canadian Standards Association, Rexdale, Ontario, Canada, 2004.

Maurenbrecher, A.H.P. 1983. Compressive strength of eccentrically loaded masonry prisms. Proceedings of the Third Canadian Masonry Symposium, Edmonton, Canada. June, pp. 10.1-10.13.

Structural Clay Products Institute. 1969. Recommended practice for engineered brick masonry. SCPI, McLean, VA.

Turkstra, C. J., and Thomas, G. R. 1978. Strain gradient effects in masonry. Proceedings, North American Masonry Conference, No. 22, 21 pp., University of Colorado, Boulder, August.

Yokel, F.Y., Mathey, R.G., and Dikkers, R.D. 1971. Strength of masonry wall under compressive and transverse loads”, Building Science Series 34, National Bureau of Standards, Washington D.C.